International Journal of Thermal Sciences 48 (2009) 1206–1212

Contents lists available at ScienceDirect

International Journal of Thermal Sciences

www.elsevier.com/locate/ijts

Impact of dissociation and end pressure on determination of laminar burning velocities in constant volume combustion

C.C.M. Luijten *, E. Doosje, J.A. van Oijen, L.P.H. de Goey

Eindhoven University of Technology, Section Combustion Technology, Department of Mechanical Engineering, P.O. Box 513, 5600 MB Eindhoven, The Netherlands

ARTICLE INFO

Article history:
Received 12 June 2008
Received in revised form 1 September 2008
Accepted 7 October 2008
Available online 8 November 2008

Keywords:
Laminar burning velocity
Constant volume combustion
Two-zone model
Multi-zone model

ABSTRACT

Determining laminar burning velocities S_L from the pressure trace in constant volume combustion requires knowledge of the burnt fraction as a function of pressure, $x(p)$. In recent literature $x(p)$ is either determined via numerical modeling or via the oversimplified assumption that $x(p)$ is equal to the fractional pressure rise. Recently, we have shown that the latter violates energy conservation, and derived alternative analytical $x(p)$ relations based on zone modeling which are more simple to apply than numerical models. However we had to assume perfect gas behavior, neglecting dissociation. In this paper we systematically compare our analytical models with a numerical two-zone model and with a 1D unsteady simulation (1DUS) of a spherical stoichiometric methane–air flame in a constant volume. Results indicate that our analytical models reasonably describe the burnt fraction as a function of fractional pressure rise. However the $x(p)$ relation also involves the (theoretical) end pressure p_e. Its value significantly affects S_L, with a relative sensitivity close to minus one, and is influenced by dissociation. Evaluating p_e from an equilibrium code, in combination with the analytical $x(p)$ model, provides S_L results within 3% accuracy. This approach removes the need for numerical modeling of intermediate stages of combustion. Still, highest accuracy for S_L is achieved using numerical $x(p)$ models that account for dissociation also for intermediate stages. Comparing results of the 1DUS with the two-zone equilibrium model shows that the combined effect of detailed chemistry, flame stretch, heat transfer between zones, and the temperature gradient in the burnt mixture is limited to about 1% for the example case.

1. Introduction

Laminar burning velocities of a combustible mixture can be obtained by recording the pressure p as a function of time in a constant volume vessel. One of the key advantages is that burning velocity values (S_L) are obtained for a range of pressures and temperatures (along an isentrope) in one single experiment. Another advantage is that only the pressure is needed to determine S_L – although observations of the flame are often made to rule out disturbances due to cracking, wrinkling or the appearance of cellular structures.

In the analysis of pressure data, a set of assumptions is commonly made, including uniformity of pressure, negligible external heat loss or gain (ignition), no buoyancy effects, isentropic compression of the unburnt gas, and an infinitely thin and spherical flame front with no heat transfer between the burnt and unburnt zones. Using these assumptions, S_L can be related to the pressure trace through a differential equation, cf. [1]:

$$\frac{\mathrm{d}p}{\mathrm{d}t} = \frac{3}{\mathcal{R}}\left(\frac{\mathrm{d}x}{\mathrm{d}p}\right)^{-1}\left[1-\left(\frac{p_i}{p}\right)^{1/\gamma_u}(1-x)\right]^{2/3}\left(\frac{p}{p_i}\right)^{1/\gamma_u} S_L. \tag{1}$$

Herein p_i is the initial pressure, γ_u the isentropic exponent of the unburnt gas, and $\mathcal{R}$ the vessel radius. Since the differential equation also contains the burnt mass fraction x, the relation between x and p must be known. Fitting the solution to an experimental pressure trace provides values of S_L, either averaged or, if desired, as a function of pressure and temperature.

In their pioneering paper [2], Lewis and von Elbe use a rather complicated procedure to obtain the burnt fraction from the pressure recording, using graphical methods (corresponding to what would be a numerical solution nowadays). Later in their textbook [3] they argue that the relation between x and p is very close to linear, and they introduce the relation

$$x = \frac{p-p_i}{p_e-p_i}. \tag{2}$$

Ever since, this relation has been used quite a lot in combination with Eq. (1).

* Corresponding author. Tel.: +31 40 2475347; fax: +31 40 2433445.
E-mail address: c.c.m.luijten@tue.nl (C.C.M. Luijten).

1290-0729/$ – see front matter
doi:10.1016/j.ijthermalsci.2008.10.006

Nomenclature

c	specific heat capacity	J kg^{-1} K^{-1}	
e	specific internal energy	J kg^{-1}	
f	function defined in Eq. (6)		
γ	specific heat ratio		
h	specific enthalpy	J kg^{-1}	
p	pressure	bar	
q	heat flux	W m^{-2}	
r	radius	m	
$\mathcal{R}$	effective vessel radius	m	
ρ	mass density	kg m^{-3}	
S	burning velocity	m s^{-1}	
σ	surface area	m^2	
t	time	s	
T	temperature	K	
u	bulk velocity	m s^{-1}	
U	diffusion velocity	m s^{-1}	
v	specific volume	m^3 kg^{-1}	
ω	chemical source term	kg m^{-3} s^{-1}	
x	mass fraction burnt		

Subscripts

b	pertaining to burnt mixture
e	final (end) condition
i	initial condition
j	species index
L	laminar
n	pertaining to nth zone
p	at constant pressure
r	relative (pressure rise)
t	total
u	pertaining to unburnt mixture
v	at constant volume

Around 1980 a new class of models appeared, pioneered by Metghalchi and Keck [4]. In these models, the equations expressing conservation of specific volume and energy are, for every incremental pressure step, solved for the burnt mass fraction x and the burnt temperature T_b. In a later paper from Metghalchi's group, Elia et al. [5] apply a similar model with multiple zones, an approach that was introduced by Bradley and Mitcheson [6], accounting for the temperature gradient in the burnt mixture. Recently, Saeed and Stone [7] also published a multi-zone model, in which they compare the evolution of pressure versus mass fraction burnt with Eq. (2). For a stoichiometric methane–air mixture, their multi-zone $x(p)$ curve lies slightly below Eq. (2) for intermediate stages of combustion.

Thus far, the zone models have always required numerical solution of the conservation equations. As a consequence, there are still many authors who prefer the simplicity and ease-of-use of the linear relation (2), as witnessed by a number of recent publications [8–13]. Obviously, such analytical approaches have clear advantages. Avoiding computational effort is one of them. Analytical relations also provide simplicity and insight, for instance, by enabling a clear analysis of limiting cases, as we will illustrate in Section 3.

Recently we have demonstrated the possibility to analytically solve the conservation equations that lie at the basis of the zone models [14]. This has resulted in new closed expressions for $x(p)$, which were found to show roughly the same deviation with respect to Eq. (2) as the numerical models. Remarkably, the $x(p)$ result did not depend on the number of zones; in particular, the two-zone result was found to coincide with the 20-zone result. Since the two-zone analytical $x(p)$ relation – expressed by Eq. (5) given in the next section – is about as simple to use as Eq. (2), we suggested that experimental S_L values based on the linear approximation should be re-evaluated using the new relation.

In the derivation of analytical relations, however, we had to assume perfect gas behavior of both unburnt and burnt gas. This implies (besides both mixtures having constant specific heats) that the average molar mass before and after combustion remains constant. Hence, shifting chemical equilibrium due to the changing temperature of successively burnt shells is not taken into account. In the present paper we systematically investigate the impact of these simplifications, by comparison with other models in which the simplifications are relieved step by step.

A second point of concern is that analytical $x(p)$ relations require the end pressure p_e as input. In practice this kind of relations is employed up to the point where heat losses become important, i.e. when the flame first touches the wall. The p_e value required in the evaluation is necessarily the theoretical end pressure (which would be achieved when a perfectly spherical and adiabatic flame would develop in a spherical vessel in the absence of gravity). In this paper we will quantitatively analyse the impact of the end pressure value on the obtained burning velocity.

Finally we will show how the combined effect of $x(p)$ model and end pressure affects the differences between S_L values, found from various models used in conjunction with Eq. (1). Throughout the paper we will use stoichiometric methane–air as an example case. In our experimental test rig we have verified that flame instabilities as mentioned above do not occur for that system and conditions as presented in this paper.

2. Theory

In this section we briefly discuss several models for $x(p)$. The linear approximation expressed by Eq. (2) will not be repeated; it is merely used as a reference for the other models – by subtracting the linear "background" from $x(p)$, differences become much better visible.

Analytical models for both two and multiple zones, which we published first in Ref. [14], are briefly described in the first two subsections. The most restrictive simplification (besides more common assumptions such as an infinitely thin flame front) is the assumption of perfect gas behavior.

The two-zone analytical model in addition neglects the burnt temperature gradient. This simplification was shown not to affect the $x(p)$ results within a perfect gas context [14]. However, when both a burnt temperature gradient *and* dissociation are allowed, this may no longer hold true: enhanced dissociation near the core of the vessel may affect the mass-averaged burnt temperature, leading to different results for $x(p)$ as well. This forms the key motivation for the present work, in which additional models are used to cross-check the results of our analytical efforts.

Two categories of additional models will be employed. First, numerical two-zone results are obtained from an in-house model; details are given in Section 2.3. Applying this model both with one-step complete combustion and with equilibrium chemistry, allows us to distinguish between the effects of temperature dependent specific heat and dissociation in the burnt mixture.

Numerical multi-zone results will not be discussed (however, they do exist for methane–air [7]). Instead, we present numerical solutions of the one-dimensional unsteady transport equations for a spherical methane–air flame at constant volume (hereafter re-

ferred to as 1DUS). This model employs full time-dependent chemistry (resulting in a finite thickness of the flame and preheat layer), with temperature dependent caloric properties for each species. Therefore this model is considered to capture most of the physics. Its results are used as reference data for the other models.

2.1. Analytical two-zone model

In a two-zone model, both the burnt and unburnt zones have uniform temperatures and compositions. Conservation of specific volume v and internal energy e are then expressed by

$$v_t = x v_b + (1-x) v_u, \tag{3}$$

$$e_t = x e_b + (1-x) e_u, \tag{4}$$

where the subscript t denotes 'total'. The specific internal energy is evaluated for the unburnt mixture as $e_u = c_{vu}(T_u - T_0) + \Delta e$ where T_0 is a reference temperature and Δe is the specific internal energy of combustion. For the burnt mixture, $e_b = c_{vb}(T_b - T_0)$. For perfect gases, the above two equations can be manipulated into a closed expression for $x(p)$. The main steps involved are elimination of T_b, and considering the limiting situation for $x \to 1$ near the end of combustion. The result is [14]:

$$x = \frac{p - p_i f(p)}{p_e - p_i f(p)}, \tag{5}$$

where $f(p)$ is defined by

$$f(p) = \frac{\gamma_b - 1}{\gamma_u - 1} + \left(\frac{\gamma_u - \gamma_b}{\gamma_u - 1}\right)\left(\frac{p}{p_i}\right)^{(\gamma_u - 1)/\gamma_u}. \tag{6}$$

Both x and its derivative (which is straightforwardly obtained from the above expressions) can be inserted into the differential equation (1), resulting in a lengthy but analytical expression that is easily evaluated, without the need for numerical solution.

By construction, the resulting expression obeys energy conservation. In Ref. [14] it is argued that this does not hold true for Eq. (2). This observation can be attributed to an underestimation of entropy production by the linear model, as we have extensively argued in a recent paper [15]. For this reason, Eq. (5) is clearly preferable over Eq. (2).

The end pressure p_e in the two-zone model is obtained from conservation of internal energy for $x = 1$:

$$c_{vu}(T_i - T_0) + \Delta e = c_{vb}(T_e - T_0). \tag{7}$$

The unburnt specific heat is evaluated at $T_i = 298.15$ K (equal to the reference temperature T_0). Specific heat of the burnt gas is evaluated at $(T_i + T_e)/2$. This choice is conceptually better than that in Refs. [14,15], where c_{vb} was evaluated at T_e, since the right-hand term in Eq. (7) stems from integration over T_0 to T_e. In both cases, this requires upfront knowledge of T_e. If desired, the values can be refined using a few iterations for T_e. In this way, the following values are obtained: $c_{pu} = 1078$ J kg^{-1} K^{-1}; $c_{vu} = 777$ J kg^{-1} K^{-1}; $c_{pb} = 1425$ J kg^{-1} K^{-1}; and $c_{vb} = 1124$ J kg^{-1} K^{-1}. The specific heat ratios follow as $\gamma_u = 1.39$ and $\gamma_b = 1.27$. The internal energy of combustion per unit mass of mixture $\Delta e = 2.76$ MJ kg^{-1}. The resulting end temperature $T_e = 2744$ K, the associated end pressure $p_e = 9.2$ bar.

2.2. Analytical multi-zone model

The approach sketched above for two zones can be extended to multiple zones. Indeed, along the same lines it is possible to derive analytical results for the burnt fraction as a function of pressure in a multi-zone setting [14]. Neglecting heat loss to the vessel wall, the conservation equations are [5]:

$$v_t = \sum_{j=1}^{n-1} x_j v_{bj} + x_n v_{bn} + \left[1 - \sum_{j=1}^{n} x_j\right] v_u, \tag{8}$$

$$e_t = \sum_{j=1}^{n-1} x_j e_{bj} + x_n e_{bn} + \left[1 - \sum_{j=1}^{n} x_j\right] e_u. \tag{9}$$

Shells are burning consecutively. At any time step, a shell with index n is just burning. Shells with lower indices have burnt previously, and are compressed isentropically during burning of the nth shell. For this reason, the terms with $j = n$ are treated differently from the others in Eqs. (8) and (9). The increment x_n in mass fraction burnt in the nth shell, together with the burnt temperature of that shell T_{bn} immediately after burning, are obtained by analytical solution of Eqs. (8) and (9), keeping track of x and T_b values of previously burnt shells [14,15]. Specific heats are taken identical as in the two-zone model. Heat exchange between zones is neglected. The total burnt fraction x after burning of N zones is given by

$$x = \sum_{n=1}^{N} x_n. \tag{10}$$

2.3. Numerical two-zone model

The numerical two-zone model starts from the same equations (3) and (4). Again heat losses are neglected. However the perfect gas assumption is dropped. Temperature dependent caloric properties are evaluated from polynomial fits, taken from a recent version of the Burcat tables [16]. The numerical model was run in two modes. In the first mode, further referred to as "no dissociation", complete combustion is assumed into CO_2 and H_2O. In the second mode, referred to as "equilibrium", the burnt gas is assumed to be in chemical equilibrium. Depending on pressure and temperature, the composition of the burnt mixture is computed using an equilibrium solver, based on Ferguson [17]. Temperature dependent equilibrium constants are taken from the JANAF tables [18]; species considered are CO_2, H_2O, N_2, O_2, CO, H_2, H, O, OH and NO.

The conservation equations are solved for x and T_b for every incremental pressure step. The pressure profile is input by the user. Temporal details of this profile are not important; since equilibrium chemistry is used, the variable time has already been eliminated from the model. Experimental pressure traces cannot be used, since these do not reach the theoretical end pressure due to heat losses near the end of combustion. The model is run until the burnt mass fraction reaches unity; the corresponding pressure at that point is the end pressure p_e associated with this model.

2.4. 1D unsteady simulation

Reference results are obtained by numerically solving the unsteady 1D partial differential equations describing conservation of mass, N species and energy:

$$\frac{\partial \rho}{\partial t} + \frac{1}{\sigma}\frac{\partial}{\partial r}(\sigma \rho u) = 0, \tag{11}$$

$$\frac{\partial \rho Y_j}{\partial t} + \frac{1}{\sigma}\frac{\partial}{\partial r}\left[\sigma \rho (u + U_j) Y_j\right] = \omega_j, \quad j = 1, \ldots, N, \tag{12}$$

$$\frac{\partial \rho h}{\partial t} + \frac{1}{\sigma}\frac{\partial}{\partial r}\left[\sigma \rho \sum_{j=1}^{N} (u + U_j) Y_j h_j + \sigma q\right] = \frac{\partial p}{\partial t}. \tag{13}$$

Since a low Mach number approximation is applied, the momentum equation can be omitted. Detailed chemistry and transport models are used for the chemical source term ω_j, species diffusion velocity U_j and heat flux q, i.e. the GRI 3.0 reaction mechanism

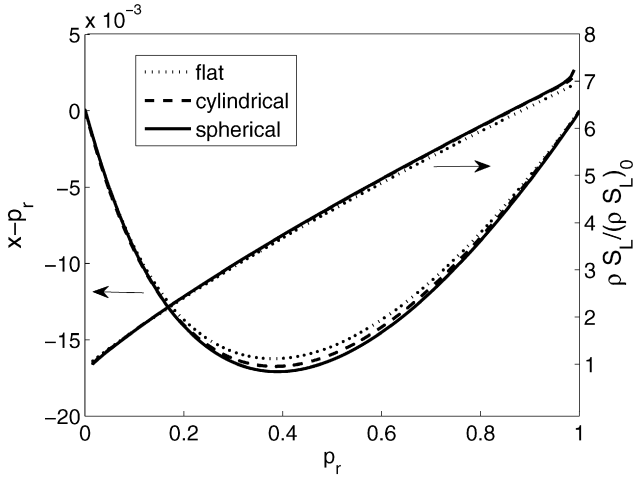

Fig. 1. Mass fraction burnt x (left axis) and normalized mass burning rate (right axis) as a function of fractional pressure rise for a 1D unsteady simulation of a confined stoichiometric methane–air flame starting at $p_i = 1$ bar and $T_i = 298$ K, for different flame geometries. Linear approximation has been subtracted from x for better visibility of differences.

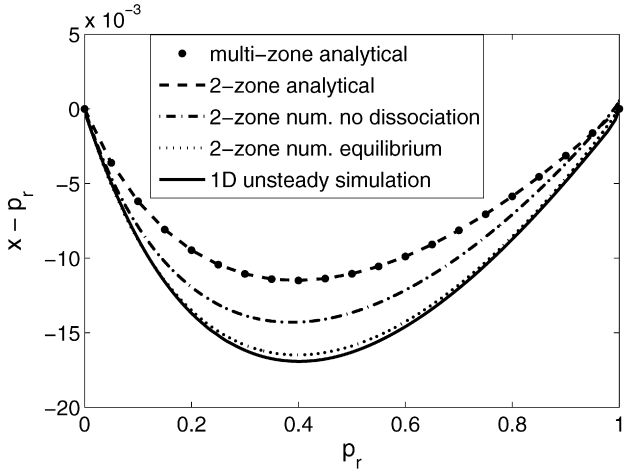

Fig. 2. Burnt mass fraction x as a function of fractional pressure rise for a spherical stoichiometric methane–air flame, for various models indicated in the legend. Linear approximation has been subtracted for better visibility of differences.

[19] and multi-component diffusion including Soret and Dufour effects. Radiation effects are neglected. The equations are discretized in space with a second order finite volume approach. Time integration is performed using a fully implicit, second order BDF (Backward Differentiation Formula) scheme with variable time stepping. The initial condition consists of the unburnt mixture in the whole domain except for a small flame kernel at the center. The influence of the ignition procedure on the results is negligible.

The 1D differential equations can describe flat, cylindrical and spherical expanding flames by applying an area σ that is proportional to the radius r to the power 0, 1, and 2, respectively. In this way, the influence of flame stretch can be investigated. In Fig. 1 (left axis), the burnt mass fraction x is shown versus fractional pressure rise, defined by

$$p_r = \frac{p - p_i}{p_e - p_i}. \tag{14}$$

The burnt mass fraction is based on the mass of methane in the volume. The end situation ($x = 1$ and $p = p_e$) is taken at the time the amount of methane has reduced to 10^{-3} times its initial value. For the spherical case, the end pressure is 8.9 bar. Different choices based on other species or smaller unburnt fractions left, result in slightly different end pressures (difference less than 0.5%), but hardly influence the $x(p)$ curves shown in Fig. 1.

The results show that for this mixture the influence of flame geometry on the $x(p)$ curve is negligible. This is consistent with assumptions made in the analytical models, since the flame geometry is not present in the conservation equations (3) and (4).

Also plotted in Fig. 1 (right axis) is the mass burning rate ρS_L, normalized by its value for a flat flame at 298 K and 1 bar. The results imply that the effect of flame stretch on the burning velocity is very small, which is to be expected since the Lewis number for methane is close to one. For other fuels, larger differences might be observed.

3. Results and discussion

In this section results for $x(p)$ and S_L are compared for various models, with the main goal of assessing the quality of the analytical models discussed above. In the expressions for x the initial pressure p_i and time resolved pressure $p(t)$ are experimentally determined. The end pressure p_e must be obtained from a computation, since it is not reached in practice. For a systematic comparison of results, it is advantageous to first analyse x as a function of fractional pressure rise p_r defined by Eq. (14). Subsequently, the impact of the end pressure p_e is discussed, the value of which differs significantly between models. Finally, Section 3.3 discusses the overall impact of the chosen $x(p)$ model and end pressure on S_L values obtained from Eq. (1).

3.1. Comparison of $x(p)$ relations

Fig. 2 shows differences between $x(p)$ and the linear relation for each of the models discussed, as a function of the fractional pressure rise p_r. This way of plotting allows zooming in on the mutual differences. The agreement between the models is encouraging. The models all show a maximum deviation around $p_r = 0.4$. Furthermore, these deviations are all about 0.014 ± 0.003 in magnitude. As already reported in Ref. [14] the perfect gas models for two and twenty zones coincide. Obviously, our analytical models are able to capture the largest part of the deviation between numerical model predictions and the linear relation. Therefore, if one wishes to evaluate burning velocity data from pressure traces without the use of a numerical model, Eq. (5) should clearly be preferred over Eq. (2).

This conclusion can also be stated as follows. The linear relation (2) forms the limiting case of Eqs. (5) and (6) for $\gamma_u = \gamma_b$. Therefore, taking into account the difference in specific heat between burnt and unburnt mixtures turns out to be far more decisive than other, more subtle effects. The latter category consists of temperature dependent specific heats, dissociation, a gradient in burnt temperature, detailed chemistry, and flame stretch (which was already discussed before with Fig. 1).

Still, significant differences remain between the analytical models and the various numerical results. The smallest difference is found with the numerical model based on one-step complete combustion ("no dissociation" in Fig. 2). Indeed, this model is very similar to the two-zone perfect gas model, the only difference being the temperature dependence of specific heats. It is noted that the difference between the models can be made smaller by evaluating the burnt specific heat at a higher temperature. This reduces γ_b, hence increases $(\gamma_u - \gamma_b)$, leading to increased deviations from the linear model. However, to guarantee an objective comparison, we evaluated c_{pb} at a temperature halfway between T_i and T_e.

Allowing for dissociation in the burnt mixture one observes that the deviation from the linear model increases. This holds for both the 1DUS model and the two-zone model assuming chemical equilibrium. Looking at the spacing of lines in Fig. 2, the impact of

dissociation appears to be about as large as the impact of temperature dependent specific heats.

Most importantly, the two models allowing for dissociation almost coincide. The main aspects in which the 1DUS differs from the numerical two-zone model are: the use of detailed chemistry; the intrinsic allowance for a gradient in burnt temperature; and the possibility of mass and heat transfer between "zones". To judge from Fig. 2, the combined result of these effects is almost negligible. This might imply that these effects are also individually unimportant, although a subtle cancelation of effects cannot be ruled out.

It is tempting to interpret the results with dissociation in terms of a difference in γ_b and γ_u, which governs the minimum in the $x(p) - p_r$ curves at least for the analytical models – an observation that can be demonstrated by an analytical exercise based on Eqs. (5) and (6). A deeper minimum in these models corresponds to a larger difference, hence one would expect a smaller γ_b for the models with dissociation. However, comparing the two-zone variants, the "equilibrium" model finds $\gamma_b = 1.25$ on average, whereas the "no dissociation" model finds $\gamma_b = 1.24$. This seems counterintuitive, but can be explained by heat being consumed by dissociation. This increases the "gross" specific heat of the burnt mixture (total energy needed to increase the temperature by 1 K), but this effect is not accounted for in the "net" specific heat, which is just the temperature derivative of the internal energy at fixed composition.

3.2. Impact of end pressure

We have seen that the general behavior of the mass fraction burnt as a function of pressure is reasonably covered by the analytical (perfect gas) models. Still, the quality of the $x(p)$ relation in an absolute sense also depends on the value of the end pressure p_e. As discussed before, Eq. (1) requires input of a *theoretical* value for p_e. This leads to an uncertainty in p_e, which translates into an error in S_L using the analytical relations. From Eq. (1) the sensitivity of S_L to errors in p_e can be derived by partial differentiation with respect to p_e, using Eqs. (5) and (6). The resulting expression is not reproduced here. The computed sensitivity $(\mathrm{d}S_L/S_L)/(\mathrm{d}p_e/p_e)$ is -1.024 ± 0.002 over the whole domain $x = [0, 1]$. For Eq. (2) this coefficient is close to -1.1 over the whole domain. So within good approximation, each percent error in p_e translates into an equal but opposite relative error in S_L.

The end pressure for each model is governed by the molar averaged temperature or, equivalently, by the mass-averaged temperature and the average molecular weight (specific gas constant) after combustion. For the two-zone models, only one burnt temperature is obtained for each pressure step. For the analytical multi-zone model and for the 1DUS, temperature profiles over the burnt mixture are obtained.

Fig. 3 shows the temperature development of each shell in the analytical multi-zone model, as a function of the total mass fraction burnt. In principle, the 1DUS provides temperature as a function of radius for different time steps; to facilitate comparison with Fig. 3, its results have been reworked into the same format (this requires coupling between time and mass fraction burnt; then, 20 "zones" are identified containing the amounts of mass for each of which the pressure rises with 5% of its total increase from p_i to p_e). Results are shown in Fig. 4.

Some features of the temperature fields in Figs. 3 and 4 are similar. The total amount of isentropic compression of the unburnt mixture is about equal, leading to an unburnt temperature slightly above 500 K just before complete combustion. The burnt temperatures during the initial phase of combustion are also quite similar (around 2300 K); they are apparently not high enough to cause significant dissociation. A computation at 1 bar and 2300 K using

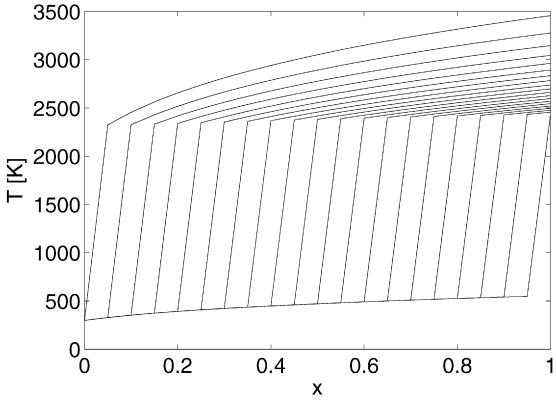

Fig. 3. Temperatures computed for individual zones using a 20-zone perfect gas model. Stoichiometric methane–air flame, starting from $p_i = 1$ bar and $T_i = 298$ K.

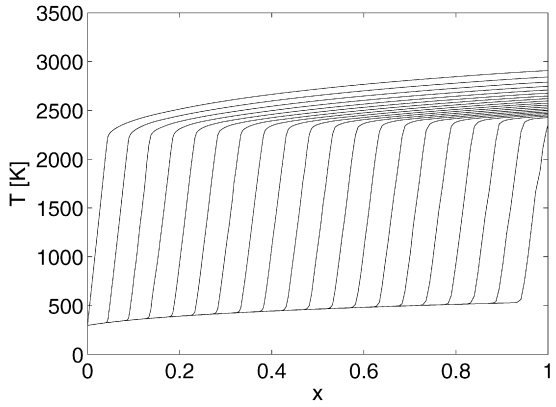

Fig. 4. Temperatures for 20 "zones" reconstructed from $T(r, t)$ profiles of 1DUS (see text). Stoichiometric methane–air flame, starting from $p_i = 1$ bar and $T_i = 298$ K.

Morley's GASEQ program [20] reveals that the CO molar fraction reaches 1.2%; all other minor species have molar fractions 0.6% (O_2) and less.

This changes during later stages of combustion. Compression of the burnt mixture in the perfect gas model leads to a final temperature gradient of about 1000 K over the vessel, whereas in the 1DUS model this is only about 500 K. The impact of dissociation clearly manifests itself in this difference: requiring chemical energy to break molecular bonds, dissociation significantly lowers the thermal energy content of the burnt mixture during later stages of combustion.

To assess the impact of the lower end temperatures resulting from dissociation, the mass-averaged burnt temperature for each model is plotted in Fig. 5. Notice that the 1DUS curve in this figure steeply bends down for small x, which is caused by the finite thickness of the flame. As expected, both models allowing for dissociation have significantly lower burnt temperatures (and smaller temperature increases) than the models assuming one-step irreversible chemistry. Again, the two-zone and multi-zone perfect gas models coincide, a consequence of the fact that only mass-averaged temperatures matter when the molecular weight remains constant.

The end pressure values for the various models are:

- Numerical two-zone, "irreversible": 9.4 bar;
- Analytical perfect gas models: 9.2 bar;
- Numerical two-zone, "equilibrium": 9.0 bar;
- 1DUS with detailed chemistry: 8.9 bar;

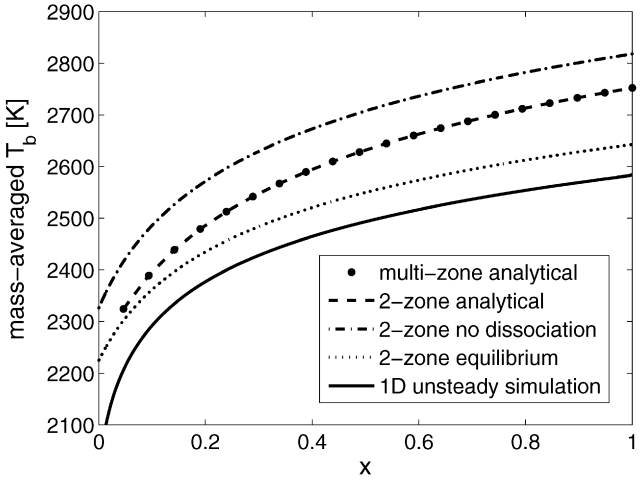

Fig. 5. Mass averaged burnt temperature as a function of mass fraction burnt. Stoichiometric methane–air flame, starting from $p_i = 1$ bar and $T_i = 298$ K.

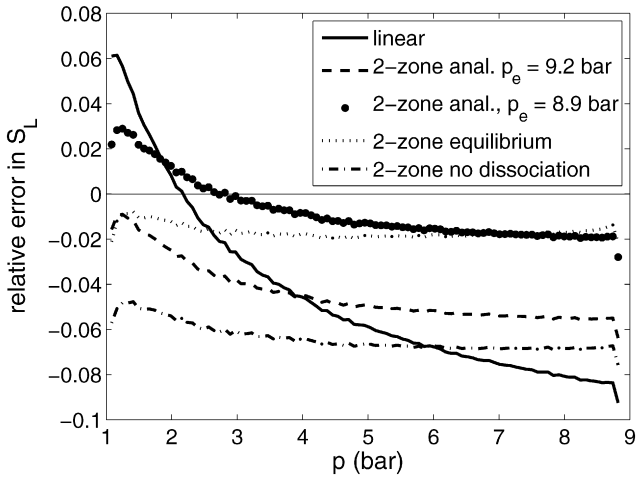

Fig. 6. Relative error in burning velocity obtained from Eq. (1) as a function of absolute pressure. The 1DUS is used as a reference for the other models.

- Numerical multi-zone model with equilibrium, from Ref. [7]: 8.7 bar;
- Equilibrium solver of Ref. [20] (for reference): 8.8 bar.

These values correlate in order with the end values of mass-averaged burnt temperatures as shown in Fig. 5. This shows that the impact of decreasing temperature on end pressure dominates that of decreasing molecular weight due to dissociation. As expected, the two-zone model with equilibrium chemistry is closest to the 1DUS value. Since the 1DUS model captures most of the real physics and chemistry, the value of 8.9 bar obtained with this model is considered most reliable. It is also very close to the equilibrium result of Ref. [20] (notice that the latter also neglects the burnt temperature gradient). Since the perfect gas end pressure is 0.3 bar higher, S_L values obtained from it would be about 3% too low for our example case, considering only the effect of end pressure.

3.3. Overall impact of $x(p)$ model on S_L

The combined impact of end pressure and $x(p_r)$ on burning velocity values obtained from Eq. (1) can be quantified as follows. For a given vessel radius and pressure trace, the factors $3/\mathcal{R}$, $\mathrm{d}p/\mathrm{d}t$ and $(p/p_i)^{1/\gamma_u}$ are equal for all models. Model dependent factors are the one in right brackets, and $\mathrm{d}x/\mathrm{d}p$. Fig. 6 shows the error in S_L, computed as the relative difference in the model dependent factors with respect to the corresponding factors for the 1DUS, so

$$\text{rel. error in } S_L = \frac{\mathcal{F}_{\text{model}} - \mathcal{F}_{\text{1DUS}}}{\mathcal{F}_{\text{1DUS}}}, \tag{15}$$

where

$$\mathcal{F} = \left(\frac{\mathrm{d}x}{\mathrm{d}p}\right)\left[1 - \left(\frac{p_i}{p}\right)^{1/\gamma_u}(1-x)\right]^{-2/3}. \tag{16}$$

Results are shown as a function of absolute pressure up to 8.9 bar, which is the pressure value in the 1DUS calculation at the moment the flame reaches the vessel wall. Multi-zone analytical results are left out, being equal to the two-zone results.

The linear relation appears to give errors up to 8%. Notably the error is quite large for small x, where the linear relation is often claimed to be correct. In a recently submitted paper we show (by taking the limit for small x) that the difference between Eqs. (2) and (5) leads to differences in S_L of a factor γ_u/γ_b. This might explain the results of Dahoe and De Goey [8], who used Eq. (2) and found burning velocities 5–10% larger than literature values. In Fig. 6 we used $p_e = 9.2$ bar for the linear model; replacing this by a more accurate value of 8.9 bar shifts the whole curve upwards, increasing the error to above 10% for small x, but decreasing the error for large x.

Errors in S_L for the analytical perfect gas model are smaller over the whole range. The magnitude of the error is limited to about 5%. For small x (where burnt temperatures are relatively low and dissociation therefore unimportant) it approaches zero. On average, the error is about −4%, which is a consequence of the end pressure used being too high. The error curve shifts up when a more realistic end pressure is used, as indicated by the dots in Fig. 6. In that case the error for large x is about 2%, at the cost of a somewhat larger error for small x. The average error over a larger x-range in that case approaches zero.

As expected, the two-zone model with equilibrium chemistry stays close to the 1DUS results over the whole pressure range, since it correctly accounts for dissociation in the burnt mixture. The overall error is limited to 2%, which is often sufficient in view of other experimental uncertainties involved (for our test rig we estimate the maximum relative error in the pressure measurement to be 2.5%). When dissociation is not allowed, the error increases to about 7%. The error in that case is quite constant with pressure, which must be a consequence of accounting for the temperature dependence of specific heat.

Overall, our results show that for determination of burning velocities to within 2%, dissociation must be accounted for. When an accuracy of 3% is sufficient our Eq. (5) can be used, with an end pressure value taken from an accurate numerical model that takes into account dissociation. This removes the need for numerical modeling of intermediate stages of combustion and hence provides a good combination of ease-of-use and accuracy, certainly in view of the typical accuracy of experimental data. Still, the validity of this approach over a large range of pressures, temperatures and fuels remains to be verified.

4. Conclusions

Evaluation of laminar burning velocities S_L from the pressure trace in constant volume combustion necessarily requires the burnt mass fraction as a function of pressure. We have presented various analytical $x(p)$ models that are more accurate than the, still widely employed, linear approximation.

Manipulation of volume and energy conservation laws for perfect gases leads to an analytical $x(p)$ relation that is as easy to implement as the linear one. However, the derivation requires the

assumption of perfect gas behavior, thus neglecting dissociation and other potentially important effects. In this paper we have systematically investigated the importance of these.

The numerical models used for comparison allowed for temperature dependent specific heats and dissociation. Both effects were shown to affect $x(p)$, with about equal magnitudes. One of these models, a one-dimensional unsteady simulation, was also used to confirm that flame stretch does not affect $x(p)$ for the example case used throughout this work, which is stoichiometric combustion of methane with air.

We have demonstrated that our new relations (5) and (6) fairly well capture the deviation from the linear relation found from the numerical models. This proves that neglect of the difference between burnt and unburnt specific heat ratios is the major pitfall of the linear approximation. Furthermore, the latter can be shown to violate energy conservation, and to give erroneous results particularly for small x, in contrast to what is often claimed. For the example case this error can be as large as 10%, depending on the end pressure value used. For these reasons, Eq. (5) is to be strongly preferred over Eq. (2).

Any analytical $x(p)$ relation requires the (theoretical) end pressure as input. Its value affects S_L, with a relative sensitivity close to minus one. End pressure values are affected by dissociation. Using our Eq. (5) with an end pressure consistent with the perfect gas assumption leads to errors in S_L up to -5%, with -4% on average. Using an end pressure from an equilibrium solver, this error can be reduced to 3% at maximum, centered around zero. This approach takes away the need for numerical modeling of intermediate phases of combustion, thus providing a useful compromise between of ease-of-use and accuracy. The validity of this approach over a range of pressures, temperatures and fuels remains to be verified.

As may be expected, highest accuracy in experimental S_L values is achieved using a numerical model that correctly accounts for dissociation throughout the experiment (i.e. not only in the final equilibrium state). Importantly, a two-zone model with equilibrium chemistry and a one-dimensional simulation with full chemistry gave very similar $x(p)$ results, with resulting S_L values differing less than 2%, which is similar to typical experimental errors in the pressure measurement. This proves that at least the combined effect of detailed (time-dependent) chemistry, heat transfer between adjacent zones, and the temperature gradient in the burnt mixture is almost negligible, although a subtle cancelation of effects cannot be fully ruled out at this point in time.

References

[1] K. O'Donovan, C. Rallis, Combust. Flame 3 (1959) 201–214.
[2] B. Lewis, G. von Elbe, J. Chem. Phys. 2 (1934) 283–290.
[3] B. Lewis, G. von Elbe, Combustion, Flames and Explosions of Gases, 2nd edition, Academic Press, New York, 1961.
[4] M. Metghalchi, J. Keck, Combust. Flame 38 (1980) 143–154.
[5] M. Elia, M. Ulinski, M. Metghalchi, Trans. ASME 123 (2001) 190–196.
[6] D. Bradley, A. Mitcheson, Combust. Flame 26 (1976) 201–217.
[7] K. Saeed, C. Stone, Combust. Theory Modelling 8 (2004) 721–743.
[8] A. Dahoe, L. de Goey, J. Loss Prev. Process Ind. 16 (2003) 457–478.
[9] A. Dahoe, J. Zevenbergen, S. Lemkowitz, B. Scarlett, J. Loss Prev. Process Ind. 9 (1) (1996) 33–44.
[10] J. Senecal, P. Beaulieu, Process Safety Progress 17 (1) (1998) 9–15.
[11] T. Skjold, B. Arntzen, O. Hansen, O. Taraldset, I. Storvik, R. Eckhoff, Process Safety and Environmental Protection 83 (2005) 151–160.
[12] P. Frijters, R. Klein-Douwel, S. Manski, L. Somers, R. Baert, in: J. Vandooren (Ed.), Proceedings of the European Combustion Meeting 2005, Louvain-la-Neuve, Belgium, 2005 (paper 71).
[13] A. Dahoe, J. Loss Prev. Process Ind. 18 (2005) 152–166.
[14] C. Luijten, L. de Goey, in: G. Skevis (Ed.), Proc. 3rd European Combustion Meeting, 2007.
[15] C. Luijten, E. Doosje, L. de Goey, Int. J. Therm. Sci. (2008), submitted for publication.
[16] A. Burcat, B. Ruscic, Ideal gas thermochemical database with updates from active thermochemical tables, available at http://garfield.chem.elte.hu/Burcat/burcat.html, 2007.
[17] C. Ferguson, Internal Combustion Engines, 1st edition, Wiley, Chichester, 1986.
[18] M. Chase, C. Davies, R. Downey Jr., JANAF thermochemical tables, 1986.
[19] G. Smith, D. Golden, M. Frenklach, N. Moriarty, B. Eiteneer, M. Goldenberg, C. Bowman, R. Hanson, S. Song, W. Gardiner Jr., V. Lissianski, Z. Qin, available at http://www.me.berkeley.edu/gri-mech/.
[20] C. Morley, A Chemical Equilibrium Program for Windows, available at http://www.gaseq.co.uk/, 2005.